Temporally disordered granular flow: A model of landslides

Bosiljka Tadić*
Jožef Stefan Institute, P.O. Box 3000, 1001-Ljubljana, Slovenia
(Received 23 September 1997; revised manuscript received 10 December 1997)

We propose and study numerically a stochastic cellular automaton model for the dynamics of granular materials with temporal disorder representing random variation of the diffusion probability $1-\mu(t)$ around threshold value $1-\mu_0$ during the course of an avalanche. Combined with the slope threshold dynamics, the temporal disorder yields a series of secondary instabilities, resembling those in realistic granular slides. When the parameter μ_0 is lower than the critical value $\mu_0^\star \approx 0.4$, the dynamics is dominated by occasional huge sandslides. For the range of values $\mu_0^\star \leq \mu_0 < 1$ the critical steady states occur, which are characterized by multifractal scaling properties of the slide distributions and continuously varying critical exponents $\tau_X(\mu_0)$. The mass distribution exponent for $\mu_0 \approx 0.45$ is in agreement with the reported value that characterizes Himalayan sandslides. At $\mu_0 = \mu_0^\star$ the exponents governing distributions of large relaxation events reach numerical values which are close to those of parity-conserving universality class, whereas for small avalanches they are close to the mean-field exponents. [S1063-651X(98)01904-7]

PACS number(s): 81.05.Rm, 64.60.Lx, 05.40.+j, 02.60.Cb

I. INTRODUCTION

Understanding flow in realistic granular materials appears to be an important problem from both a practical and a theoretical point of view [1,2]. Renewed theoretical interest in this field has concentrated on the origin of scaling that characterizes phenomena in slowly driven granular materials: distributions of avalanches in realistic granular piles [3–8], stratification [9], compactification [10], etc. The central question is as follows: Do granular piles self-organize into critical steady states [1] and if so, under what conditions? Another interesting phenomenon related to dynamics of granular materials in nature is the landscape evolution due to overland and channel flow, which results in fractal topography. The underlying mechanisms of erosion with spatially and temporally varying erosion rates are the subject of intensive discussion in the literature [11].

It has been understood that realistic flow in slowly driven granular piles depends on many parameters, such as shapes and sizes (and masses) of individual beans, roughness of contact surfaces, their wetting properties, etc. Random (or controlled) variations in some of these parameters lead to fluctuations of contact angles and force distribution [12], nonlinear friction, stochastic character of diffusion, velocity and convection directions, and fluctuations in angle of repose. Unidirectional flow—reflecting dependence on gravity—is common in all granular materials, as is the occurrence of secondary avalanches following the initial instability. Molecular dynamic (MD) simulations [13] and various cellular automata models with stochastic relaxation rules [14–16] have been useful in describing certain aspects of realistic granular flow. However, comparison with measured avalanche properties has been only qualitative.

In experiments the most often measured quantity is the outflow current J, which is defined as the number of grains that leave the system when an avalanche hits its lower boundary. The probability distribution of outflow current $P(J)$ in the steady state obeys the scaling form $P(J,L) = L^{-\beta}\mathcal{G}(JL^{-\nu})$ with $\beta = 2\nu$ when the linear size L of the pile support is varied, as found in Ref. [4] for sandpiles of relatively small sizes. Using silicon dioxide sand Rosendahl *et al.* [5] concluded that small and large avalanches behave differently and the distribution $P(J)$ shows no simple finite-size scaling. Moreover, avalanche statistics was found to vary with the size of grains used. Measuring the *internal* avalanches Bretz *et al.* [6] have also observed that two types of statistics are governing small and large avalanches. The measured distribution of avalanche size exhibits a power-law behavior $D(s) \sim s^{-\tau_s}$ with [6] $\tau_s \approx 2.14$, which probably applies for avalanches of small sizes. The two time (and size) scales were more clearly demonstrated recently by MD simulations [13], leading to two exponents $\tau_s = 2$ for short, and $\tau_s = 1.5$ for long time scale. A sophisticated measurement of the internal avalanches was done with a one-dimensional ricepile [7], in which elongated rice grains were used to suppress inertial effects. Scaling properties of the distribution of dissipated energy were determined, indicating that details of the dissipation are responsible for the occurrence of the critical state. In another experiment the transport of *individual* grains was monitored, and the distribution of transit time was also found to exhibit robust scaling behavior [8].

The collected data for the landslides in nature, triggered by various mechanisms, also exhibit a power-law behavior [1]. The exponents for the area of slides have been estimated in the range $\tau_s = 1.16 - 2.25$ [17], depending on the dominating triggering mechanism and region where the data were collected. The distribution of the mass collected from Himalayan sandslides is characterized by the exponent $\tau_m = 0.19 - 0.23$ [18].

In the present work we introduce a new stochastic model of directional flow on the two-dimensional square lattice in

*Electronic address: Bosiljka.Tadic@ijs.si

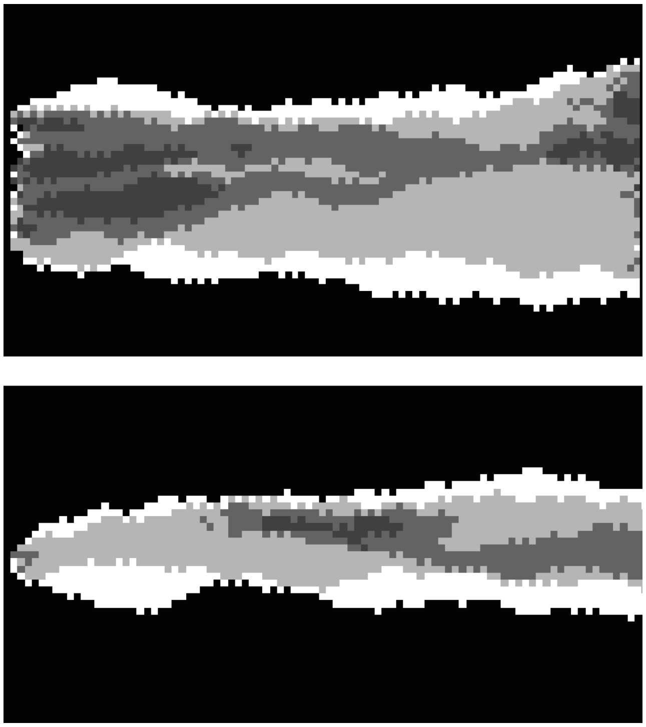

FIG. 1. Two examples of avalanches running from left to right: (below) in the scaling region $\mu_0 > \mu_0^\star$ and (top) in the region of erosional avalanches. Multiple topplings up to fourth order are marked by different degrees of gray color.

which numerous after-avalanches are generated within a certain correlation time due to temporal disorder in the diffusion term. The dynamic rules are a combination of stochastic diffusion and deterministic branching processes. The diffusion probabilities change *randomly in time*, but are space independent. Fluctuations in diffusion probability $1-\mu(t)$ around threshold value $1-\mu_0$, which depends on external conditions and thus appears as a control parameter, is motivated by fluctuations in wetting and drying conditions *after an avalanche commenced* (see Sec. II). Notice that the lifetime of an avalanche can range from seconds in the laboratory granular piles to geological times in the landscape evolution. Therefore, the change of local stability conditions during the avalanche lifetime is a natural choice in the case of long relaxation times. A similar type of disorder in directed percolation processes was recently considered by Jensen [19].

We perform extensive numerical simulations for various values of the parameter μ_0 and lattice sizes L, and quantify the behavior by the landslide distributions of: (i) duration t—time that an instability lasts measured on the internal time scale; (ii) size s—area affected by an instability, and (iii) mass n—number of grains that exhibit slides during one avalanche, and (iv) by outflow current J—number of grains that fall off the open boundaries of the pile. Self-organized critical states are found for a range of values of the control parameter $\mu_0 \geq \mu_0^\star \approx 0.4$, which are characterized with multifractal scaling properties and μ_0-dependent critical exponents. For $\mu_0 < \mu_0^\star$ large discharging events occur occasionally, representing large-scale erosional reorganization of the system rather than fluctuations around a well-defined critical state.

The organization of the paper is as follows: In Sec. II we introduce the model and show two representative examples of landslides. The probability distributions of slides and their scaling properties are determined in Secs. III and IV for various values of the linear system size L and the parameter μ_0 in the scaling region. Section V contains a short summary and the discussion of the results.

II. MODEL AND LANDSLIDES

We consider a square lattice oriented downward, with a dynamic variable, height $h(i,j)$, associated to each site. The relaxation rules are a combination of (i) stochastic diffusion by two particles when $h(i,j) \geq h_c$ with probability $\mu(t)$, which varies in time (see below), and (ii) deterministic convection, when local slope $\sigma(i,j) \equiv h(i,j) - h(i+1,j_\pm)$ exceeds some critical value $\sigma(i,j) \geq \sigma_c$. At each site the rule (ii) is applied by toppling one particle along an unstable slope repeatedly until both local slopes drop below σ_c. The system is updated in parallel, which leads to a well-defined internal time scale of the relaxation process. The updating is stopped when *all* affected sites become temporarily stable. Here $(i+1,j_\pm)$ are positions of two downward neighbors of the site (i,j). Mass flow is always downward, however, the instability can propagate backwards both due to nonlocal slope condition and due to time-dependent diffusion probability. We assume that diffusion probability fluctuates stochastically in time, but is space independent. Implementation of this rule is done as follows: We preset the threshold value μ_0, which is the same for all sites in the system. Then at each site that is affected by an avalanche a new value $\mu(t)$ is selected at each time step until the avalanche stops from a set of random numbers evenly distributed on the interval (0,1), and toppling is accepted if $\mu(t) \leq \mu_0$, and rejected otherwise [20]. Therefore, for $\mu_0 = 1$ all sites topple (the rule becomes deterministic), whereas for $\mu_0 < 1$ an unstable site might not topple at a given time t because of instantly low diffusion probability $p(t) \equiv 1 - \mu(t) < 1 - \mu_0$, however, it may topple at a later time step $t' > t$ if $p(t')$ exceeds the threshold diffusion probability $1-\mu_0$. This temporally varying disorder mimics changes in sticking properties with time, which then locally influence the angle of repose. This phenomenon can be of interest for the flow of granular materials with large effective friction, such as ricepiles [7] in which the effects of granular boundaries may depend on the local dynamic variable $h(i,j)$ and its derivatives. Therefore the difference $\mu(t) - \mu_0$ is a measure of the dynamic friction. Recently proposed models with stochastic critical slope rules in one dimension [15] proved very successful in describing the observed *transport* properties of ricepiles [8]. Whereas for *avalanche* distributions these models predict universal scaling exponents, in contrast to the experimental observations [3,5–7].

Another interesting example is represented by landscape evolution, which can also be considered as a granular flow [1], in which local wetting properties fluctuate in time. By wetting, $p(t)$ drops below the threshold diffusion probability $1-\mu_0$, the grains stick together, and the system builds up large local slopes. At a later time t' these slopes may become unstable either when due to drying $p(t')$ exceeds the threshold, or when the slopes become larger than critical. Two

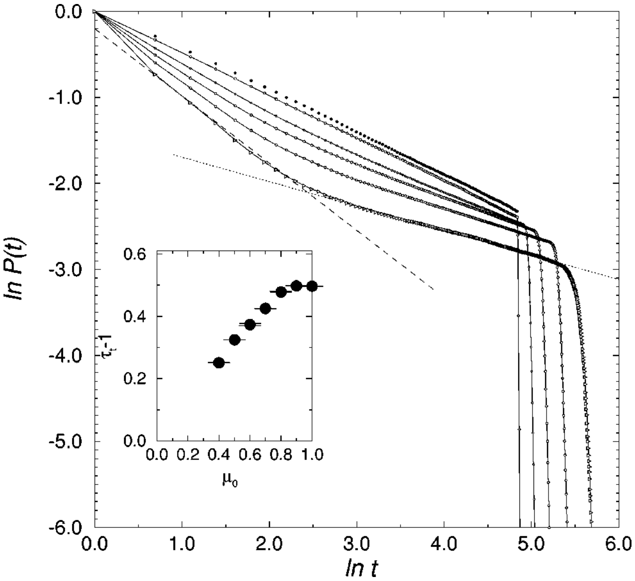

FIG. 2. Double-logarithmic plot of the integrated probability distribution of avalanche durations $P(t)$ vs duration t for $L=128$ and various values of the control parameter $\mu_0=1$, 0.9, 0.8, 0.7, 0.6, and 0.5 (top to bottom). Dashed and dotted lines indicate slopes of small and large avalanches, respectively. Inset: Scaling exponent of large avalanches τ_t-1 vs μ_0.

different classes of triggering mechanisms of landslides have been discussed in the literature [21]: rainfall and water level, which control soil moisture on one side, and ground motion, which leads to slope variation on the other. The values of measured exponents of landslide distributions are directly related to the locally prevailing triggering mechanism [17]. In principle, threshold shear stress may depend on the slope angle and on soil properties, which are influenced by soil moisture. We assume that these two mechanisms are related *dynamically*. In the present model both mechanisms are effective: The soil moisture, which affects local height, varies stochastically in time at each site, whereas we assume that the shear stress threshold depends only on the local angle and thus remains deterministic. Moreover, by tuning the critical height mechanism via the parameter μ_0, we find nonuniversal critical properties and a transition to noncritical dynamic states, in qualitative agreement with experimental observations. A different model of landslides is obtained by ''averaging out'' the critical height mechanism and assuming stochastic variations of critical slope, which can be viewed as one of few possible generalizations of stochastic critical slope models [15] to two dimensions. So far the results of two-dimensional stochastic critical slope models are not available in the literature [22].

The system is perturbed by adding grains one at a time at a random site on the first row, thus increasing local height and slopes. Therefore, an instability (avalanche) can in principle start only from the top, however, secondary avalanches are commencing from any affected site in the system, triggered either by a high instant value of $\mu(t)$ or by supercritical slope. In order to have ''clean'' statistics, we start each avalanche from the top row and consider only those secondary avalanches that are *spatially connected* within a certain correlation time t_c. Here t_c is not a prefixed parameter, but it is determined by the relaxation process itself. Typically t_c is determined by the lifetime of the instability, thus $t_c \gg 1$ for large relaxation events. There are two interesting limits of our model. In the limit $\mu_0=1$ it reduces to the deterministic directed model [23], whereas for $\mu_0<1$ and in the limit when the correlation time is *strictly* equal to one, it reduces to the model considered in Ref. [16].

The temporally varying diffusion probability is a new ingredient of our model, which was not considered so far in CA models of granular flow. It appears to be responsible both for new scaling properties and for the transition into the state dominated by large erosional avalanches. In Fig. 1 are shown two examples of simulated landslides with multiple topplings due to secondary avalanches up to fourth degree in the scaling region (bottom) and a large erosional event (top).

III. PROBABILITY DISTRIBUTIONS OF SLIDES AND THEIR SCALING PROPERTIES

In this section we present results of numerical simulations of avalanche statistics. As discussed in Sec. I, a landslide consists of many interpenetrating avalanches of different degree, which are spatially connected to one another within the lifetime of the instability. For concreteness, the probability distributions are determined for the *whole* relaxation event, which is equally termed as avalanche and/or landslide. We apply open boundary conditions in the perpendicular direction (see also later an example where periodic boundaries have been used). In most simulations we used $h_c=2$ and $\sigma_c=8$. By varying the external parameter μ_0 between 0 and 1 and lattice size L between 12 and 192, we determine the distributions of size, mass, and duration of avalanches (slides).

In Figs. 2 and 3 the distributions of avalanche duration longer than t, $P(t)$, size larger than s, $D(s)$, and mass larger than n, $D(n)$, are shown for $L=128$ and various values of the parameter μ_0. [Notice that in the deterministic limit $\mu_0=1$ the distributions $D(s)$ and $D(n)$ become identical, however, unbounded number of topplings at each site for $\mu_0<1$ leads to two distinct distributions.] For $\mu_0<1$ a characteristic behavior with two scales appears: the steep section corresponding to small avalanches, and the flat section to large avalanches. The crossover length between small and large relaxation events varies with μ_0, however, it remains small (cf. Figs. 2 and 3), so that distributions of avalanches smaller than the crossover length extend only over one decade. Here we concentrate on the behavior of large avalanches (i.e., avalanches that are larger than the crossover

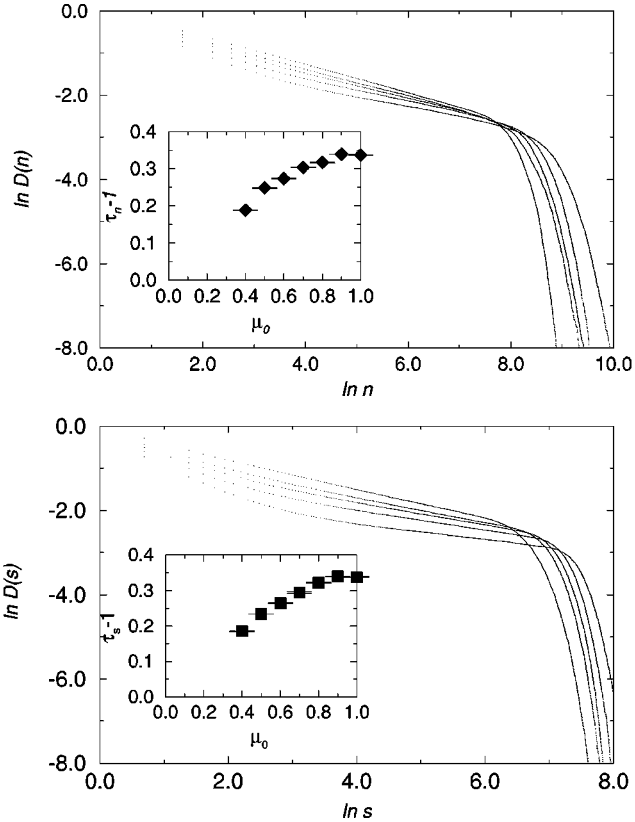

FIG. 3. Double-logarithmic plot of the integrated probability distribution of avalanche size $D(s)$ vs size s (bottom) and mass $D(n)$ vs n (top), for $L=128$ and for (top to bottom) $\mu_0=1$, 0.8, 0.7, 0.6, and 0.5 . Inset: Scaling exponent of large avalanches τ_s-1 vs μ_0 (bottom figure) and τ_n-1 vs μ_0 (top figure).

length). With lowering the threshold diffusion probability μ_0 a large number of secondary instabilities develop, leading to the flattening of the distributions. However, we find a power-law behavior $P(t)\sim t^{1-\tau_t}$, $D(s)\sim s^{1-\tau_s}$, and $D(n)\sim n^{1-\tau_n}$, as long as $\mu_0\geqslant 0.4$. The exponents τ_t, τ_s, and τ_n appear to vary continuously with control parameter μ_0, as shown in the insets to Figs. 2 and 3. The character of the dynamics changes below $\mu_0^\star\approx 0.4$, where only occasionally very large avalanches occur. We study in some more detail the relaxation clusters at $\mu_0=0.4$. Numerical values of the exponents are $\tau_t=1.253$, $\tau_s=1.202$, and $\tau_n=1.190$ for the distributions of duration, size, and mass of avalanches, respectively. In addition, we have measured the distribution of linear elongation of avalanches in the direction of transport $P(\ell)\sim\ell^{-\tau_\ell}$, the mass-to-scale ratio with respect to parallel length $\langle s\rangle_\ell\sim\ell^{D_\parallel}$, and the average transverse extent $\langle\ell_\perp\rangle\sim\ell^{\zeta}$. We find $\tau_\ell=1.578$, $D_\parallel=1.572$, and $\zeta=D_\parallel-1=0.572$ (estimated error bars ± 0.03). These values are close to the numerical values of the exponents in the parity-conserving universality class [24] of branching processes. On the other hand, the exponents governing small events increase with decreasing μ_0 (cf. Fig. 2), reaching the values $\tau_t^s=1.92$, $\tau_s^s=1.67$, and $\tau_n^s=1.45$ for the duration, size, and mass of small avalanches, respectively, at $\mu_0=\mu_0^\star$. Notice that although the scale of the distributions is small, being bounded by the crossover length, these values of the exponents indicate closeness of the mean-field universality class.

Multifractal scaling properties of landslide distributions

By varying the lattice size L with μ_0 fixed in the scaling region we study the finite-size effects on the distributions of avalanches. In contrast to most of the two-dimensional sandpile automata models in the literature, the present distributions do not obey simple finite-size scaling. Instead, we find that *different regions of a large avalanche have different fractal properties* and consequently their own exponents. The following multifractal scaling form [25];

$$P(X,L)\sim(L/L_0)^{\phi_X(\alpha_X)}, \tag{1}$$

with

$$\alpha_X\equiv\left(\ln\frac{X}{X_0}\right)\Big/\left(\ln\frac{L}{L_0}\right) \tag{2}$$

fits well our data with $L_0=1/4$ and $X_0=1/4$. (Here $X\equiv t,s,J$). In Figs. 4 and 5 we show the probability distributions of duration and size, respectively, for five different lattice sizes L and for fixed $\mu_0=0.7$. The corresponding spectral functions $\phi_t(\alpha_t)$ versus α_t and $\phi_s(\alpha_s)$ versus α_s are shown in the insets to Figs. 4 and 5.

IV. OUTFLOW CURRENT

The outflow current results only from those avalanches that reach an open boundary of the system. The size of such events and their frequency is a relative measure of the transport processes that occur in the interior of the pile. The outflow current is easy to measure both in laboratory experiments and in natural landslides. For instance, the width of the sedimented layers of granular materials that occur below steep sections in mountains are directly related to the size of outflow avalanches from that section. Sensitivity of the outflow current distribution $P(J)$ to variations in the control parameter is monitored in our model for $L=48$ with periodic

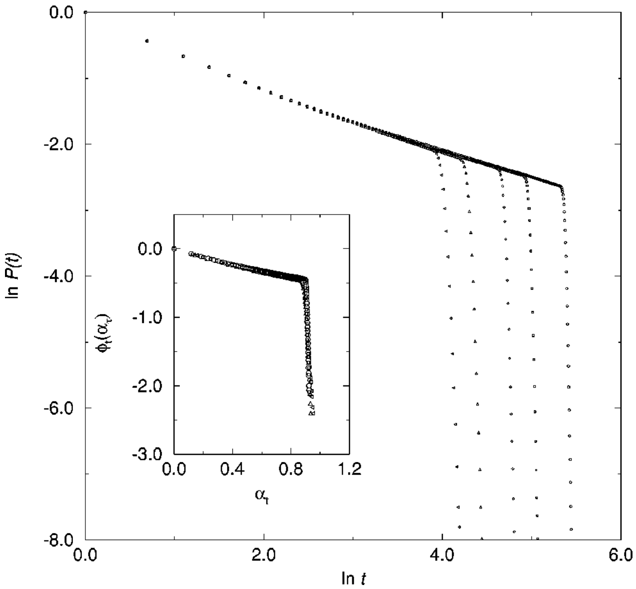

FIG. 4. Double-logarithmic plot of the distribution $P(t)$ vs t for $\mu_0=0.7$ and for various lattice sizes $L=12$, 24, 48, 96, and 192 (left to right) with open boundary conditions. Inset: Multifractal scaling function $\phi_t(\alpha_t)$ vs α_t.

boundary conditions in the perpendicular direction. In Fig. 6 we show the distribution $P(J)$ versus J for $\mu_0=1$, 0.8, 0.6, 0.4, and 0.2. Once again, the change in the character of the dynamics below $\mu_0^\star$ is also seen in the outflow current, which becomes centered around a certain mean value (depending on the lattice size). Above $\mu_0^\star$, we find that the outflow current distribution exhibits multifractal scaling properties according to Eqs. (1) and (2). The results for $\mu_0=0.7$ and varying L from 12 to 192, obtained for open boundary conditions in perpendicular direction, are shown in Fig. 7.

Additional information about transport processes in the interior of the system is obtained by measuring the outflow current as a function of time, and time intervals between successive outflow events. In the inset to Fig. 6 we show the average time interval between outflow events as a function of the control parameter μ_0. The time intervals grow exponentially on lowering μ_0. In Fig. 8 the outflow current is shown as a function of time (measured on the external time scale, i.e., by the number of added particles), averaged over 1000 time steps for $L=54$ and with periodic perpendicular boundary conditions. For $\mu_0 \geqslant 0.4$ (cf. lower three panels), the outflow current fluctuates around mean value $J_0=1$, thus balancing the input current and maintaining the steady states of the system (a steady state is characterized by balance between input and output currents). The amplitude of the outflow events increases with decreasing μ_0, and at the same time the frequency of events decreases. This behavior is consistent with the histogram that is shown in Fig. 6. The character of the dynamics changes for $\mu_0<\mu_0^\star$ (see top panel in Fig. 8), with dominating output events of large size and large time intervals between the events. At $\mu_0=\mu_0^\star$ a dynamic phase transition occurs between critical steady states above $\mu_0^\star$ and states without long-range correlations below $\mu_0=\mu_0^\star$. (Similar phase transitions are found also in Refs. [16] and [26], however, in different universality classes.) Although for $\mu_0<\mu_0^\star$ the system is likely to build up a finite slope (unlimited piling is prevented by the deterministic critical slope rule), preliminary results show that a substantial growth of the average slope occurs only for $\mu_0<0.2$,

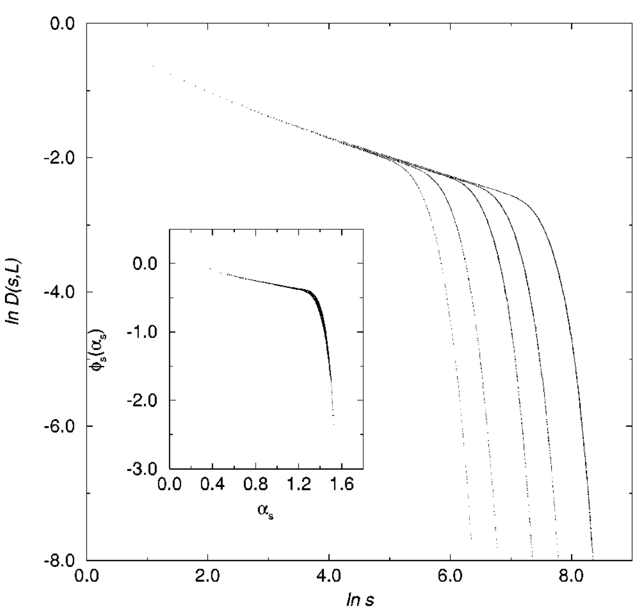

FIG. 5. Double-logarithmic plot of the distribution of sizes $D(s)$ vs s for the same set of parameters as Fig. 4. Inset: Multifractal scaling function $\phi_s(\alpha_s)$ vs α_s.

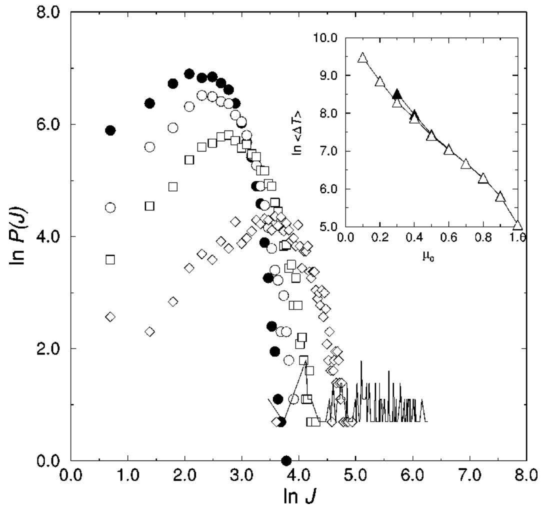

FIG. 6. Double-logarithmic plot of the probability distribution of outflow current $P(J)$ vs J for $L=48$ with periodic boundary conditions in perpendicular direction, and for $\mu_0=1$, 0.8, 0.6, 0.4, and 0.2 (top to bottom). Inset: Average time intervals between outflow events on the same lattice for $\sigma_c=8$ (open triangles) and $\sigma_c=4$ (filled triangles).

reaching the value σ_c at $\mu_0 \to 0$. Further work is necessary in order to investigate the universality class of this phase transition.

V. DISCUSSION AND CONCLUSIONS

In the present model, combined relaxation rules with temporal disorder are responsible for numerous after-avalanches, which lead to large relaxation events resembling sandslides in realistic granular materials. Numerical simulations show that such large relaxation events exhibit scaling behavior for a range of values of the control parameter $\mu_0 \geqslant \mu_0^\star \approx 0.4$. The avalanche distributions are characterized by continuously varying scaling exponents, in qualitative agreement with the data collected from natural landslides. Moreover, comparison of the exponent of the avalanche mass distribution τ_n for $0.4<\mu_0<0.5$ with the one that characterizes Himalayan sandslides reported in Ref. [18] is satisfactory. For various lattice sizes the distributions are characterized by multifractal rather than finite-size scaling properties. The deterministic part of the relaxation rules leads to branching processes with, on the average, even number of offsprings. For this reason the scaling exponents for the distributions reach numerical values characteristic of the modulo-two conserving processes (also known as parity-conserving processes) before scaling behavior disappears at $\mu_0=\mu_0^\star$. Below $\mu_0^\star$ the *critical* steady state is lost. The dynamics is dominated by large erosional avalanches in a region close to $\mu_0^\star$ and a net average slope appears for smaller values of μ_0.

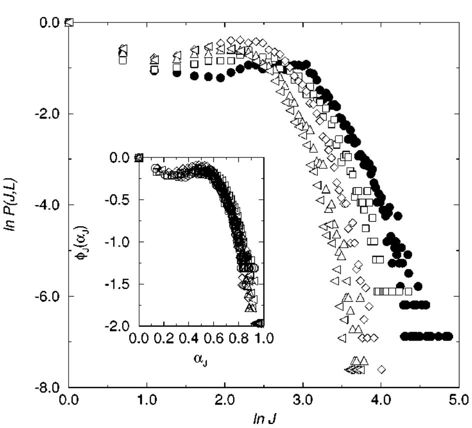

FIG. 7. Distribution of outflow current measured with open boundary conditions for various lattice sizes $L=12$, 24, 48, 96, and 192 (left to right) and for fixed $\mu_0=0.7$. Inset: Spectral function $\phi_J(\alpha_J)$ vs α_J.

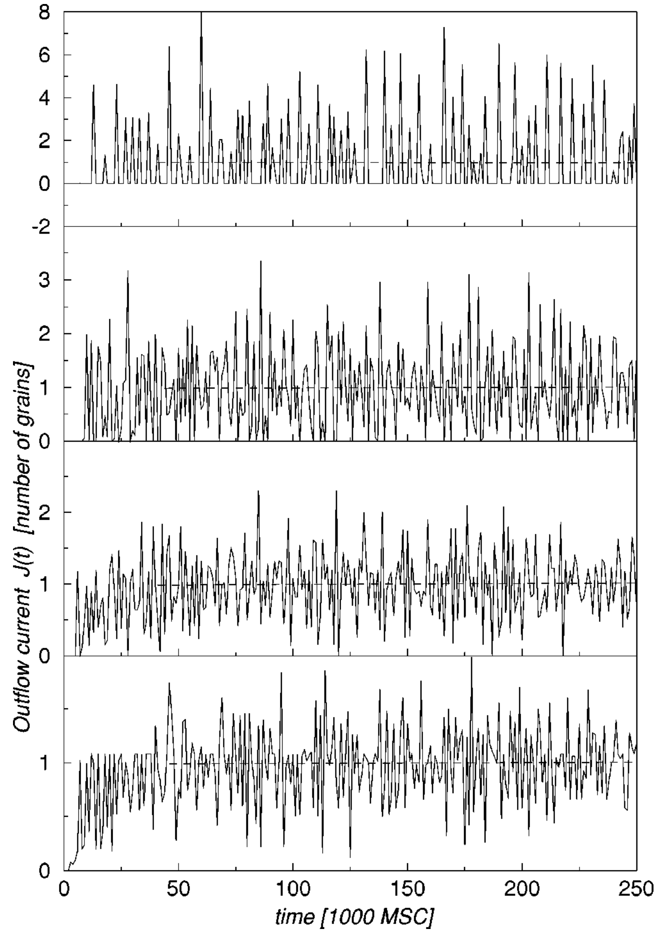

FIG. 8. Outflow current $J(t)$ vs time t (measured in number of added particles), averaged over 1000 time steps, for $L=54$ and $\mu_0=1$, 0.7, 0.4, and 0.3 (bottom to top) and with periodic boundary conditions. Dashed lines are mean values calculated by linear fits of the data for $t>40$: (bottom to top) 0.9972, 1.0004, 0.9935, and 0.9892. Slopes of the dashed lines are smaller than 10^{-5} in each case.

ACKNOWLEDGMENTS

This work was supported by the Ministry of Science and Technology of the Republic of Slovenia. I would like to thank R. Pastor-Satorras, A. Corral, and D.L. Turcotte for helpful discussions.

[1] P. Bak, *How Nature Works*, (Copernicus Springer-Verlag, New York, 1996), and references therein.
[2] H. M. Jeager, S. R. Nagel, and R. P. Behringer, Phys. Today **49**(4), 32 (1996).
[3] H. M. Jeager, C.-h. Liu, and S. R. Nagel, Phys. Rev. Lett. **62**, 40 (1989).
[4] G. A. Held, D. H. Solina, D. T. Keane, W. J. Haag, P. M. Horn, and G. Grinstein, Phys. Rev. Lett. **65**, 1120 (1990).
[5] J. Rosendahl, M. Vekić, and J. Kelly, Phys. Rev. E **47**, 1401 (1993); J. Rosendahl, M. Vekić, and J. E. Rutledge, Phys. Rev. Lett. **73**, 537 (1994).
[6] M. Bretz, J. B. Cunningham, L. P. Kurczynski, and F. Nori, Phys. Rev. Lett. **69**, 2431 (1992).
[7] V. Frette, K. Christensen, A. Malte-Sørensen, J. Feder, T. Jøssang, and P. Meaking, Nature (London) **379**, 49 (1996).
[8] K. Christensen, A. Corral, V. Frette, J. Feder, and T. Jøssang, Phys. Rev. Lett. **77**, 107 (1996).
[9] H. A. Makse, S. Havlin, P. Ch. Ivanov, P. R. King, S. Prakash, and H. E. Stanley, Physica A **233**, 587 (1996); H. A. Makse, P. Cizeau, and H. E. Stanley, Phys. Rev. Lett. **78**, 2398 (1996).
[10] M. Nicodemi, A. Coniglio, and H. J. Herrmann, e-print cond-mat/9606097.
[11] For a recent review see J. D. Pelletier, e-print, physics/970533, and references therein; See also E. Somfai, A. Czirók, and T. Vicsek, J. Phys. A **27**, L757 (1994).
[12] C.-h. Liu, S. R. Nagel, D. A. Schester, S. N. Coppersmith, S. Majumdar, O. Narayan, and T. A. Witten, Science **269**, 513 (1995).
[13] S. Sen and S. Pal, Physica A **233**, 77 (1996).
[14] E. J. Ding, Y. N. Lu, and H. F. Ouyang, Phys. Rev. A **46**, R6136 (1992); H. F. Ouyang, Y. N. Lu, and E. J. Ding, Phys. Rev. E **48**, 2413 (1993); C. P. C. Prado and Z. Olami, Phys. Rev. A **45**, 665 (1992); B. Tadić and R. Ramaswamy, Physica A **224**, 188 (1996).
[15] See Ref. [8] and L. N. Amaral and K. B. Lauritsen, Phys. Rev. E **54**, R4512 (1996); **56**, 231 (1997).
[16] S. Lübeck, B. Tadić, and K. D. Usadel, Phys. Rev. E **53**, 2182 (1996).
[17] D. L. Turcotte (unpublished).
[18] D. A. Noever, Phys. Rev. E **47**, 724 (1993). Notice that the original data were collected by clearing the mountain roads, indicating that the reported exponent applies for the integrated probability distribution of mass.
[19] I. Jensen, Phys. Rev. Lett. **77**, 4988 (1996).
[20] Notice that in this implementation the width of the distribution of $\mu(t)$ does not appear as a tunable parameter.
[21] J. D. Pelletier, D. Malamud, T. Blodget, and D. L. Turcotte, e-print physics/9705035.
[22] A. Corral (private communication).
[23] D. Dhar and R. Ramaswamy, Phys. Rev. Lett. **63**, 1659 (1989).
[24] Recently two other dynamical models in the parity-conserving universality class were reported in chemical reactions [M. H. Kim and H. Park, Phys. Rev. Lett. **73**, 2579 (1994)] and in damage spreading processes [H. Hinrichen and E. Domany, e-print cond-mat/9701011].
[25] In connection with sandpile automata the multifractal scaling was found so far in one-dimensional models: L. P. Kadanoff, S. R. Nagel, L. Wu, and S. Zhu, Phys. Rev. A **39**, 6524 (1989); B. Kutnjak-Urbanc, S. Havlin, and H. E. Stanley, Phys. Rev. E **54**, 6109 (1996); V. B. Priezzhev and K. Sneppen, *ibid.* (to be published). For a theoretical analysis of multifractal properties of sequences of transit times in the ricepile model, see R. Pastor-Satorras, Phys. Rev. E **56**, 5284 (1997).
[26] B. Tadić and D. Dhar, Phys. Rev. Lett. **79**, 1519 (1997).